A Bistable Model of Cell Polarity

Matteo Semplice[1], Andrea Veglio[2], Giovanni Naldi[3]*, Guido Serini[4], Andrea Gamba[5,6,7]

1 Department of Physics and Mathematics, Università dell'Insubria, Como, Italy, 2 Genomes and Genetics Department, Unit Physics of Biological Systems, Institut Pasteur, Paris, France, 3 Department of Mathematics "F. Enriques", Università degli studi di Milano, Milano, Italy, 4 Laboratory of Cell Adhesion Dynamics, Institute for Cancer Research and Treatment and Department of Oncological Sciences, School of Medicine, Università degli studi di Torino, Candiolo, Italy, 5 Department of Mathematics, Politecnico di Torino, Torino, Italy, 6 Laboratory of Systems Biology, Institute for Cancer Research and Treatment, Candiolo, Italy, 7 INFN, Torino, Italy

Abstract

Ultrasensitivity, as described by Goldbeter and Koshland, has been considered for a long time as a way to realize bistable switches in biological systems. It is not as well recognized that when ultrasensitivity and reinforcing feedback loops are present in a spatially distributed system such as the cell plasmamembrane, they may induce bistability and spatial separation of the system into distinct signaling phases. Here we suggest that bistability of ultrasensitive signaling pathways in a diffusive environment provides a basic mechanism to realize cell membrane polarity. Cell membrane polarization is a fundamental process implicated in several basic biological phenomena, such as differentiation, proliferation, migration and morphogenesis of unicellular and multicellular organisms. We describe a simple, solvable model of cell membrane polarization based on the coupling of membrane diffusion with bistable enzymatic dynamics. The model can reproduce a broad range of symmetry-breaking events, such as those observed in eukaryotic directional sensing, the apico-basal polarization of epithelium cells, the polarization of budding and mating yeast, and the formation of Ras nanoclusters in several cell types.

Competing Interests: The authors have declared that no competing interests exist.

* E-mail: giovanni.naldi@unimi.it

Introduction

Cell polarity plays a fundamental role in cell biology. Many cellular systems use polarity not only to respond to external stimuli but also to define tissue and organ boundaries, or to proliferate. Eukariotic cells show an extraordinary ability of orienting toward sources of chemical signals through a complex mechanism of cell membrane polarization governing the early stages of chemotaxis [1–3]. Budding yeast undergoes polarized growth during budding and mating. Epithelial cells polarize into an apical and a basolateral region.

Cell polarization can be guided by internal or external spatial cues, such as internal landmark proteins or chemoattractant signals. Many cells polarize in order to migrate in response to external cues. For example, when presented with a gradient of chemoattractant, neutrophils, neurons, budding yeast and Dictyostelium respond with highly oriented polarity and motility towards the source of chemoattractant. This behavior is exhibited for a shallow gradient of chemoattractant. Several basic stages are required for highly oriented polarity. In fact, cells rearrange cellular components leading to the development of separate leading and trailing edges with distinct sensitivities for chemoattractant. Polarization can also occur randomly in the absence of such cues, by a spontaneous symmetry breaking mechanism [4]. For example, even when stimulated by a spatially uniform concentration of chemoattractant, neutrophils and Dictyostelium cells can break their initial symmetry, acquire distinct leading and trailing edges and start to migrate randomly [5].

Polarity corresponds to the formation of regions characterized by different concentrations of specific signaling molecules. We can consider these regions as "signaling domains" being in different "chemical phases". A natural and general way to partition the cell plasmamembrane into regions characterized by complementary chemical phases is to couple local bistability with lateral diffusion [1,2]. Bistability is ubiquitous in cell signaling networks, often leading to binary outcomes in response to graded stimuli [6–10]. The role of local bistability in clustering, and in the spatial localization of activated molecules, has however started to be appreciated only recently [1–3,11–13].

Here we provide a simple, solvable model of cell membrane polarization based on the coupling of membrane diffusion with bistable enzymatic dynamics. Moreover, we show that the model can reproduce a broad range of symmetry-breaking events, such as those observed in eukaryotic chemotaxis, epithelial morphogenesis, and yeast polarization.

Results

Our general model of chemical cell membrane polarization is an abstraction of features observed in several biological systems, where a couple of interconverting signaling molecules Φ^+, Φ^- are localized on the cell plasmamembrane and are transformed into each other by a couple of counteracting enzymes X, Y (Fig. 1). The X, Y enzymes shuttle between the cytosol and the plasmamembrane, and may be activated either by a signal S coming from the environment, or by the Φ^+, Φ^- molecules themselves through local reinforcing feedback loops. The diffusivity of the X, Y enzymes in the cytosolic reservoir is much larger than lateral mobility of molecules on the cell membrane. Therefore, an approximate equilibrium is established between the population of bound enzymes
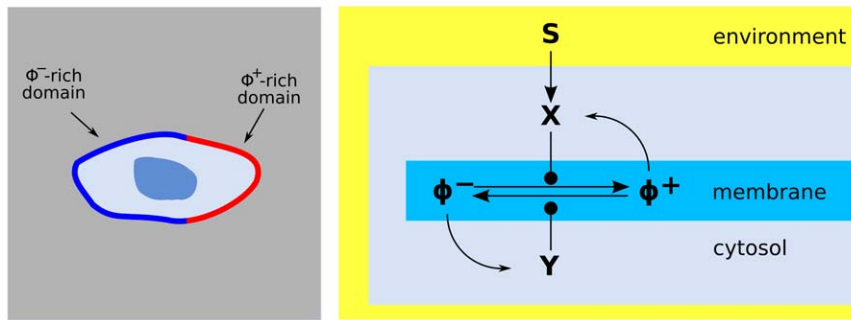
Figure 1. Prototypical model of cell polarization. A system of receptors S transduces an external distribution of chemotactic cues into an internal distribution of activated enzymes X, which catalyze the switch of a signaling molecule Φ from an unactivated state Φ^- to an activated state Φ^+. A counteracting enzyme Y transforms the Φ^+ state back into Φ^-. The network contains a couple of amplifying feedback loops: the signaling molecule Φ^- activates Y and Φ^+ acvivates X. The signaling molecules Φ^+, Φ^- are permanently bound to the cell surface S and perform diffusive motions on it, while the X, Y enzymes are free to shuttle between the cytosolic reservoir and the membrane. The result of the polarization process is the formation of separate domains with Φ^--rich patches and, respectively, Φ^+-rich patches.
doi:10.1371/journal.pone.0030977.g001

and the pool of free enzymes diffusing in the cytosolic reservoir. For instance, X and Y may represent a phosphatase-kinase couple that control the transition of a signaling molecule between two phosphorylation states.

In known biological models of cell membrane polarity, three-dimensional (3D) cytosolic diffusion takes place on characteristic times of the order of 1 s, which are much faster than the characteristic times $\sim 100\,\mathrm{s}$ implied in two-dimensional (2D) polarization dynamics [2]. This *timescale separation* implies that the 3D distribution of cytosolic molecules can be assumed to be approximately uniform in space and slowly varying in time on the characteristic timescales of 2D polarization.

The generic microscopic picture encoded in Fig. 1 can be naturally described by means of a discrete reaction-diffusion stochastic dynamics. The dynamics is essentially confined to the cell surface since, due to timescale separation, the cytosol may be described simply as an unstructured reservoir of molecules in approximate equilibrium with the chemical factors bound to the plasmamembrane. At larger length scales, a smoother mean-field dynamics described by concentration fields emerges from the microscopic interactions of individual molecules. The mean-field dynamics can be described by an appropriate partial differential equation (PDE) model and studied with analytical and numerical methods.

Here we describe the microscopic model, derive its mean-field description, study its qualitative behavior, and compare the modeling results with available experimental data. This way, we set up a general model of chemical phase separation correctly reproducing the dynamics of cell polarization in different biological models.

Microscopic model

Membrane polarization is a spatially distributed process characterized by stochasticity, excitability [14], and the coupling of the 2D dynamics of membrane-bound molecules with the 3D cytosolic dynamics. The process can be conveniently described by using a lattice approximation, *i.e.* by representing the cell membrane as a 2D lattice with sites populated by discrete amounts of molecules, while reactions and diffusive jumps are realized as stochastic processes according to the rules of chemical kinetics. The coupling to the cytosol is described by allowing shuttlying of molecules between the 2D lattice and an unstructured reservoir representing the 3D cytosolic volume. From the stochastic process we then derive a macroscopic *mean field* model, where populations of

molecules are described by continuous density fields, and their stochastic fluctuations are encoded into effective "noise" terms [12].

Each site i of the 2D lattice is populated by a discrete number of molecules of the relevant chemical factors. The probability distribution P of the molecule population evolves in time according to standard master equations taking into account all possible chemical conversions and diffusion jumps [15]. For instance, the process of conversion between Φ^+ and Φ^- signaling molecules on the i-th lattice site is described by the following terms of the master equation (see Fig. 1):

$$
\begin{aligned}
&\frac{\partial}{\partial t} P\left(n_{\Phi^+}^{(i)}, n_{\Phi^-}^{(i)}, n_X^{(i)}, \ldots\right) \\
&= W_{\Phi^+ \to \Phi^-}^{(i)}\left(n_{\Phi^+}^{(i)} + 1, n_{\Phi^-}^{(i)} - 1, \ldots\right) P\left(n_{\Phi^+}^{(i)} + 1, n_{\Phi^-}^{(i)} - 1, n_X^{(i)}, \ldots\right) \\
&\quad + W_{\Phi^- \to \Phi^+}^{(i)}\left(n_{\Phi^+}^{(i)} - 1, n_{\Phi^-}^{(i)} + 1, \ldots\right) P\left(n_{\Phi^+}^{(i)} - 1, n_{\Phi^-}^{(i)} + 1, n_X^{(i)}, \ldots\right) \\
&\quad - \left[W_{\Phi^+ \to \Phi^-}^{(i)}\left(n_{\Phi^+}^{(i)}, \ldots\right) + W_{\Phi^- \to \Phi^+}^{(i)}\left(n_{\Phi^+}^{(i)}, \ldots\right)\right] P\left(n_{\Phi^+}^{(i)}, n_{\Phi^-}^{(i)}, n_X^{(i)}, \ldots\right) \\
&\quad + \cdots
\end{aligned}
$$

where $n_M^{(i)}$ is the number of molecules of type M on lattice site i, and $W_{(reaction)}^{(i)}$ is the transition rate for the given *reaction* on site i. Moreover, we assume that a pool of N_{X_f}, N_{Y_f} free molecules X_f, Y_f populates the cytosol. A complete list of reaction and transition rates of the signaling network described in Fig. 1 is given in Table 1. X molecules activated by the external signal S via receptors are denoted by the symbol X', while X molecules activated via the feedback loop are denoted by the symbol X'' (Fig. 1). Diffusion of the Φ^+ and Φ^- molecules on the cell membrane surface is represented by jumps from a site i to a neighboring site j with rate DN/A, where D is the diffusivity, A is cell membrane area, and N is the number of lattice sites. Diffusion of the X and Y enzymes on the cell membrane is neglected. Enzymatic reaction rates are approximated by Michaelis-Menten terms.

Mean-field model

In the mean-field approximation, molecule distributions are described by continuous concentration fields, and stochasticity is encoded into an effective noise term [15]. Concentration fields are approximations to averages of molecule numbers over small

Table 1. Reactions belonging to the signaling pathway of Fig. 1 and corresponding transition rates W.

Reaction	$W^{(i)}_{forward}$	$W^{(i)}_{backward}$
$S + X_f \underset{k'_d}{\overset{k'_a}{\rightleftharpoons}} X'$	$k'_a n^{(i)}_S N_{X_f}$	$k'_d n^{(i)}_{X'}$
$\Phi^+ + X_f \underset{k''_d}{\overset{k''_a}{\rightleftharpoons}} X''$	$k''_a n^{(i)}_{\Phi^+} N_{X_f}$	$k''_d n^{(i)}_{X''}$
$\Phi^- + Y_f \underset{k_d}{\overset{k_a}{\rightleftharpoons}} Y$	$k_a n^{(i)}_{\Phi^-} N_{Y_f}$	$k_d n^{(i)}_Y$
$X' + \Phi^- \overset{k'_c}{\rightarrow} X' + \Phi^+$	$k'_c \dfrac{n^{(i)}_{X'} n^{(i)}_{\Phi^-}}{K' + n^{(i)}_{\Phi^-}}$	
$X'' + \Phi^- \overset{k''_c}{\rightarrow} X'' + \Phi^+$	$k''_c \dfrac{n^{(i)}_{X''} n^{(i)}_{\Phi^-}}{K'' + n^{(i)}_{\Phi^-}}$	
$Y + \Phi^+ \overset{k_c}{\rightarrow} Y + \Phi^-$	$k_c \dfrac{n^{(i)}_Y n^{(i)}_{\Phi^+}}{K + n^{(i)}_{\Phi^+}}$	

We denote by N_{X_f} and N_{Y_f} the number of free X, Y molecules available in the cytosolic reservoir, by $n^{(i)}_{X'}$ the number of X molecules on site i that are activated by the external signal S via receptors, by $n^{(i)}_{X''}$ the number of X molecules on site i that are activated via the feedback loop in Fig. 1.
doi:10.1371/journal.pone.0030977.t001

neighborhoods $B(r)$ of points r on the cell membrane surface:

$$m(r) = \frac{1}{surf B(r)} \sum_{i \in B(r)} n^{(i)}_M$$

and it is assumed that the size of the neighborhood is larger than the typical molecule size, but much smaller than the typical size of the cell. Low occupation numbers $n^{(i)}_M$ correspond to higher relative fluctuations around the mean-field concentration m.

From the spatially distributed signaling pathway of Fig. 1, Table 1, we derive the following mean-field equations:

$$\partial \phi^+ / \partial t = D \Delta \phi^+ + g(\phi^+, \phi^-, x', x'', y) \quad (1)$$

$$\partial \phi^- / \partial t = D \Delta \phi^- - g(\phi^+, \phi^-, x', x'', y) \quad (2)$$

$$\partial x' / \partial t = k'_a s X_f - k'_d x' \quad (3)$$

$$\partial x'' / \partial t = k''_a \phi^+ X_f - k''_d x'' \quad (4)$$

$$\partial y / \partial t = k_a \phi^- Y_f - k_d y \quad (5)$$

$$dX_f/dt = -\frac{1}{V} \int_{membrane} \frac{\partial (x' + x'')}{\partial t} d(surface) \quad (6)$$

$$dY_f/dt = -\frac{1}{V} \int_{membrane} \frac{\partial y}{\partial t} d(surface) \quad (7)$$

where Δ is a Laplace-Beltrami operator [16] representing diffusion on the cell surface, d(surface) is the area element on the cell membrane surface A, V is the cell volume, and

$$g(\phi^+, \phi^-, x', x'', y) = k'_c \frac{x' \phi^-}{K' + \phi^-} + k''_c \frac{x'' \phi^-}{K'' + \phi^-} - k_c \frac{y \phi^+}{K + \phi^+} \quad (8)$$

describes the enzymatic conversion of Φ^+ and Φ^-.

Thermal and chemical reaction noise can be taken into account by adding the corresponding randomly fluctuating terms in the right hand side of (1–7) [15].

Local equilibria

At equilibrium, the distribution of membrane-bound enzymes is "slaved" to the surface distribution of receptors and of Φ^+, Φ^- molecules (cf. 3–5):

$$x' = \frac{X_f}{k'_d / k'_a} s, \quad x'' = \frac{X_f}{k''_d / k''_a} \phi^+, \quad y = \frac{Y_f}{k_d / k_a} \phi^-, \quad (9)$$

while the amount of free cytosolic enzymes is a decreasing function of the *total* numbers of activated receptors and Φ^+, Φ^- molecules (cf. 3–7):

$$X_f = \frac{X_T}{1 + (k'_a / k'_d)\theta s_{ave} + (k''_a / k''_d)\theta \phi^+_{ave}},$$
$$Y_f = \frac{Y_T}{1 + (k_a / k_d)\theta \phi^-_{ave}}. \quad (10)$$

Here $m_{ave} = \frac{1}{A} \int_A m \, d(surface)$ denotes the average of the molecule distribution m over the cell membrane surface A, and $\theta = A/V$ is the factor needed to convert surface concentrations (measured in m^{-2}) into volume concentrations (measured in m^{-3}).

Finally, the total amount of Φ^+ and Φ^- is conserved (cf. 1–2), then

$$\phi^+ + \phi^- = c = const \quad (11)$$

Effective potential

Timescale separation implies that the equilibria (9, 10) for x', x'', y, X_f, Y_f are reached in much faster time than the equilibria for the surface distributions ϕ^+, ϕ^- of signaling molecules. This fact suggests a convenient way to study the dynamic of cell membrane polarization, namely to substitute the fast variables x', x'', y in equations (1, 2) with their steady state expressions (9, 10). The rationale here is that the concentrations (9, 10) are approximately stationary on timescales which are much shorter than the typical timescales of ϕ^+, ϕ^- variation, and slowly vary on longer timescales. This procedure coincides with the *quasi steady state approximation* used for instance in the derivation of Michaelis-Menten laws from the theory of the transition state [17].

By using the conservation law (11) we are finally reduced to consider the dynamics of *a single relevant degree of freedom*

$$\phi = \phi^+ - \phi^-$$

which obeys the dynamic equation

$$\frac{\partial \phi}{\partial t}(r, t) = D \Delta \phi(r, t) + V'(\phi) \quad (12)$$

with:

$$V'(\phi) = (c^2 - \phi^2) \cdot$$
$$\left[\frac{2(k'_c k'_a / k'_d) X_f s}{(2K' + c - \phi)(c + \phi)} + \frac{(k''_c k''_a / k''_d) X_f}{2K'' + c - \phi} - \frac{(k_c k_a / k_d) Y_f}{2K + c + \phi} \right] \quad (13)$$

(see Fig. 2). In what follows, we will assume for simplicity $K = K' = K''$. For slowly varying X_f, Y_f, equation (12) can be written in the variational form [18]:

$$\frac{\partial \phi}{\partial t}(\mathbf{r}, t) = -\frac{\delta \mathcal{F}[\phi]}{\delta \phi(\mathbf{r}, t)} \quad (14)$$

with

$$\mathcal{F}[\phi] = \int_{membrane} \left[\frac{D}{2} (grad\phi)^2 + V(\phi) \right] d(\text{surface}) \quad (15)$$

showing that the dynamics of the signaling field ϕ tends to minimize $\mathcal{F}$, which plays the role of an *effective energy functional*.

It is worth observing here that $\mathcal{F}$ does not measure the actual energy consumed by chemical reactions, but is just a convenient mathematical bookkeeping tool which allows to determine the direction of catalytic and diffusion processes taking place in any given point on the membrane surface, at any given instant of time.

Solutions of equation (12) are obtained from

$$V'(\phi) = 0, \quad (16)$$

which, once solved, gives two stable equilibrium values $\varphi_+ = c$, φ_- and one unstable equilibrium φ_u. The values φ_+, φ_- correspond to distinct, stable, uniform chemical phases, enriched respectively in the signaling molecules Φ^+ and Φ^-. We refer to the existence of two distinct stable chemical phases as *bistability*. The explicit concentration values are

$$\varphi_u, \varphi_- = \frac{1}{2} \left[-(S + T + c) \pm \sqrt{(S + T - c)^2 - 8KS} \right] \quad (17)$$
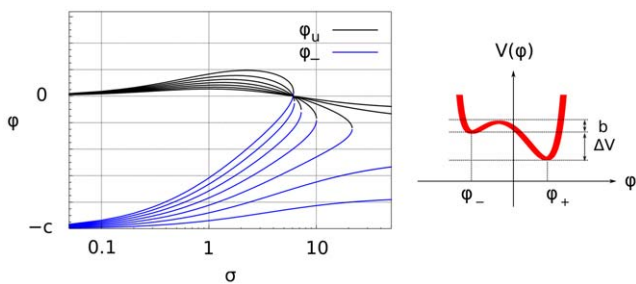
Figure 2. Stable chemical phases. Left: relative concentrations of signaling molecules in the stable chemical phase ϕ_- and unstable chemical phase ϕ_u, as a function of the renormalized activation signal σ (19) (black) and for different values of the saturation constant κ. Right: Behavior of the potential $V(\phi)$, as a function of the phase ϕ, see (13). The potential V has two minima: the left-hand one corresponding to a stable φ_--rich and the right-hand one corresponding to a stable φ_+-rich phase. The two phases are separated by an effective energy barrier. The existence of the two distinct stable chemical phases is called bistability.
doi:10.1371/journal.pone.0030977.g002

where

$$S = \frac{c\rho\sigma}{\rho + 1}, \quad T = \frac{\rho - 1}{\rho + 1}(2\kappa + 1)c, \quad \kappa = \frac{K}{c}, \quad (18)$$

with

$$\rho = \left(\frac{k''_c k''_a k_d}{k_c k_a k''_d} \right) \frac{X_f}{Y_f}, \quad \sigma = 2 \left(\frac{k'_c k'_a k''_d}{k''_c k''_a k'_d} \right) \frac{s}{c}. \quad (19)$$

Eqs. (17–19) show that the concentration values (17) are completely controlled by the *enzyme ratio* ρ, which measures the relative strength of the counteracting X and Y enzymes, and by the *renormalized activation signal* σ.

A graph of the concentration values in the two stable phases is given in Fig. 2. An important consequence of the existence of two distinct, locally stable phases is that different regions of the cell membrane can be occupied by different phases, giving rise to patterning into distinct *signaling domains*.

Patterning is possible only if the enzyme ratio ρ lies in the *bistability region* shown in Fig. 3 (see Supplementary Material Text S1). The enzyme ratio ρ may therefore also be called a *bistability parameter* for the pathway of Fig. 1.
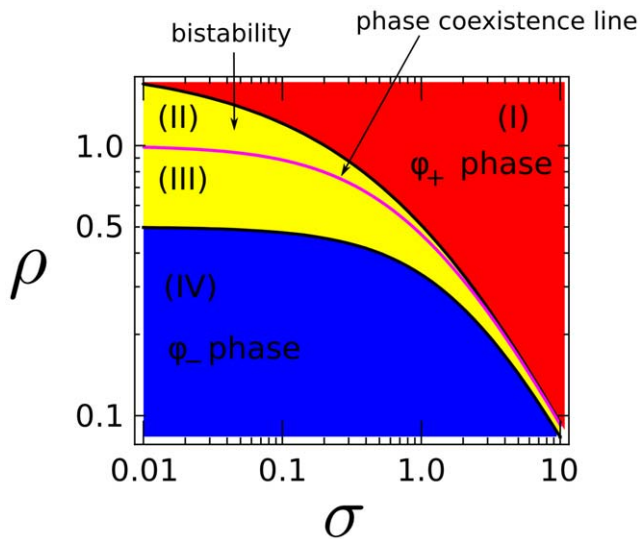
Polarity

The cell membrane is *polarized* when it is divided into two complementary regions, stably occupied by one of two distinct chemical phases, separated by a thin diffusive interface. Stable polarized equilibria are reached when the effective energy $\mathcal{F}$ is minimal, *i.e.* when both terms in Eq. (15) take on their minimal values. If *e.g.* $V(\varphi_+) < V(\varphi_-)$, no polarized configuration can be stable because the energy can still decrease by extending the area covered by the φ_+ phase, which has lower energy than the φ_- phase. The same is true if $V(\varphi_+) > V(\varphi_-)$. Therefore, stability of polarized equilibria (or *phase coexistence*) is possible only if the following mathematical condition is satisfied:

$$\Delta V = V(\varphi_+) - V(\varphi_-) = \int_{\varphi_-}^{\varphi_+} V'(\phi) d\phi = 0 \quad (20)$$

Equations (13, 20) together provide an integral equation for the value at equilibrium of the enzyme ratio ρ_{eq} (see Supplementary Material Text S1), that can be solved numerically to determine the *phase coexistence line* $\rho = \rho_{eq}$ (Fig. 3).

The second condition for energy minimization is that the square gradient term in Eq. (15) is minimized. The main contribution from this term comes from the interface between regions occupied by uniform distributions of the φ_+ and φ_- phase: energy minimization implies therefore minimization of the length of the interface that separates the two phases. The minimal value for the interface length is obtained when the cell membrane is polarized in two complementary caps, separated by a circular interface.

In the equilibrium state $\rho = \rho_{eq}$, the circular patches occupied by the φ_+ and φ_- phases have areas A_+ and A_- determined by the integral constraints (10). The two areas can be explicitly computed if the size of the interfacial region separating the two patches is negligible with respect to the cell size (Fig. 4 and Supplementary Material Text S1). For small values of the stimulation σ, patches of the φ_+ and φ_- phase are mainly sustained by positive feedback loops, while for large values of σ, they are mainly sustained by receptor activity. The two regimes correspond to the two asymptotic plateaux appearing in Fig. 4, respectively for small and large values of the stimulation σ. It is

Figure 3. Bistability region, yellow region (II)-(III), as a function of the level of external renormalized stimulation σ **for** $\kappa = 1$. The purple line corresponds to phase coexistence (polarization) and is an attractor for the polarization dynamics. The two stable domains, blue (IV) and red (I), correspond to the two φ_- and φ_+ stable phases.
doi:10.1371/journal.pone.0030977.g003

worth observing here that on two plateaux the areas of the signaling patches are almost *insensitive* to the absolute value of the external stimulation σ, in agreement with experimental observations ([19], Fig. 3).

Nucleation of signaling patches

The evolution from a quiescent state towards polarized equilibria involves a complex dynamics of nucleation and competitive growth of signaling patches. Similar processes have been known for a long time in the physics of materials [20,21].

Let us assume that in the quiescent state, the plasmamembrane is uniformly occupied by the φ_- phase (Fig. 3, region II). By switching on a strong enough external stimulation field at initial time, the plasmamembrane can be brought out of chemical
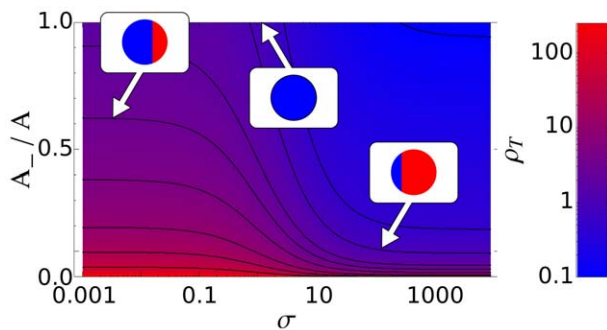
Figure 4. In the equilibrium state the circular patches occupied by the φ_+ **and** φ_- **phases have areas, respectively,** A_+ **and** A_-**.** Here we show the ratio A_-/A at different values of the stimulation σ. Curves are plotted from top to bottom with increasing ratio of the initial enzymes quantities X_T/Y_T. Each curve shows two plateaux that are approximatively independent of the signal σ. For small σ the system is dominated by the mutual interaction between Φ^+ and Φ^-, i.e., by the feedback loop, whilst for large σ the system is dominated by the interaction with receptors, i.e., by the external signal.
doi:10.1371/journal.pone.0030977.g004

equilibrium, making the φ_+ phase energetically more favorable than the φ_- phase. The energetic barrier b between the two potential wells (see Fig. 2) blocks however the continuous transition of the φ_- phase into the φ_+ phase. The transition can take place only by the formation of sizable initial germs of the φ_+ phase, driven by random thermal and/or chemical processes. Actually, small germs are mainly destroyed by diffusion, while germs larger than a critical size $r_c \propto 1/\Delta V$ expand in the φ_- sea with a front velocity $\propto \Delta V$ [1,20,22]. The larger the barrier b, the longer the waiting time for the first appearance of a sizable germ of the φ_+ phase.

Once the first sizable germ appear, the transition towards the φ_+ phase is initially limited only by the velocity of front propagation $\propto \Delta V$. However, the growth of the φ_+ phase implies depletion of the cytosolic X population, repletion of the cytosolic Y population, and decrease of ΔV, *cf.* equations (10, 13, 19). Thus, the process of growth of the φ_+ phase slows down as time advances. The cytosolic reservoir of X and Y enzymes works here as a negative feedback control that drives the plasmamembrane towards the phase coexistence line (Fig. 3) and makes polarization possible.

As soon as the plasmamembrane is driven towards the phase coexistence line, the potential difference ΔV decreases and the critical radius r_c gets larger, so that patches that were previously growing fall below the critical size r_c and start shrinking. Thus, large patches grow at the expense of smaller patches until a single patch survives. This kind of competitive growth of patches has been known for a long time in the physics of materials as *Lifshitz-Slyozov coarsening* [2,3,20,21]. The corresponding dynamics may be understood via a simple physical analogy with the nonequilibrium process taking place during the formation of precipitate from a supersaturated solution (see Fig. 5). At initial time, the concentration of some molecule ϕ is higher than the critical value ϕ_c, so that a small fluctuation, or an impurity, can easily give rise to the formation of small germs of precipitate. Germs larger than a critical size $r_c \sim (\phi - \phi_c)^{-1}$ grow steadily, while germs smaller than r_c are dissolved by diffusion. As the size of the germs grows, the molecule ϕ is extracted from the hydrated phase and transferred to the solid phase, moving the concentration ϕ closer to the critical value ϕ_c, increasing the value of r_c, and correspondingly slowing down the process of germ growth. Grains that were initially larger than r_c are dissolved, so that larger grains grow at the expense of the smaller grains. Eventually, an equilibrium is reached when $\phi = \phi_c$ and a single large grain of precipitate survives.

Robustness

An important result of the mathematical theory of phase ordering processes [20] guarantees that the scenario described in the previous paragraph does not depend on details such as the precise values of reaction and diffusion rate constants, on the identity of the individual biochemical factors, or on the precise analytical expressions derived from the law of mass action, but only on the following set of *robust properties* of the signaling network [2,3,20].

1. *Single relevant concentration field:* The polarization state of the cell membrane can be described in terms of a single relevant concentration field ϕ, while the values of other concentration fields can be derived by approximate equilibrium relations. The evolution equation for ϕ can be expressed in terms of an effective energy potential $V(\phi)$.

2. *Bistability:* Feedback loops embedded in the signaling network allow for the realization of distinct, locally stable chemical phases, separated by a potential energy difference ΔV.
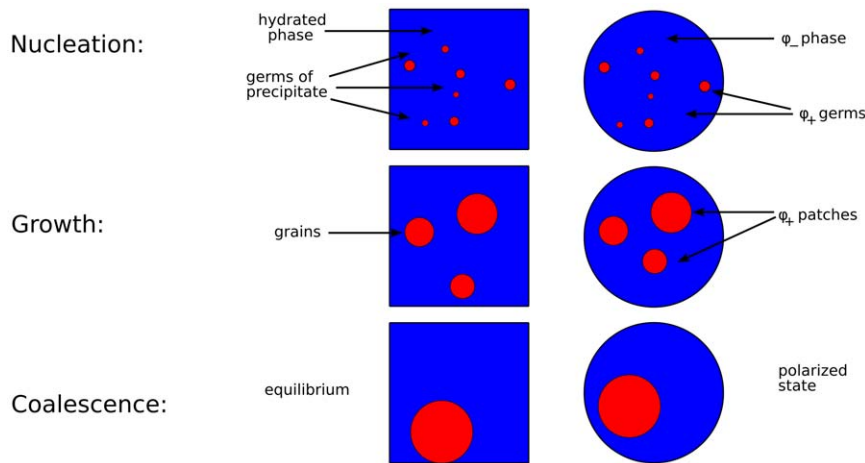
Figure 5. Physical analogy: membrane polarization and precipitation from a supersaturated solution. At initial time, the concentration of some molecule ϕ is higher than the critical value ϕ_c, so that a small fluctuation, or an impurity, can easily give rise to the formation of small germs of precipitate. Germs larger than a critical size r_c grow steadily, while germs smaller than r_c are dissolved by diffusion. As the size of the germs grows, the molecule ϕ is extracted from the hydrated phase and transferred to the solid phase, moving the concentration ϕ closer to the critical value ϕ_c, increasing the value of r_c, and correspondingly slowing down the process of germ growth. Grains that were initially larger than r_c are dissolved, so that larger grains grow at the expense of the smaller grains. Eventually, an equilibrium is reached when $\phi = \phi_c$ and a single large grain of precipitate survives.
doi:10.1371/journal.pone.0030977.g005

3. *Self-tuning:* A global feedback mechanism drives the energy difference ΔV to zero, thus bringing the plasmamembrane towards the coexistence of the two chemical phases.

The robustness of our approach has important implications.

First of all, it suggests that polarization phenomena observed in distant biological models can be described mathematically in a unified way since they share a set of common features.

Secondly, it implies that robust quantitative results can be independent on the detailed knowledge of a majority of microscopic details. This property cannot be underestimated in the study of biological phenomena where the relative abundances of biochemical factors, their interactions and reaction rates are often known with comparatively poor accuracy.

Eukariotic chemotaxis

Experiments with Dictyostelium cells exposed to uniform concentrations of cyclic AMP (cAMP) reveal a complex dynamics of membrane polarization into signaling domains enriched in either phosphatidinositol bisphosphate (PIP2) or trisphosphate (PIP3) [19]. Two enzymes, phosphatidylinositol 3-kinase (PI3K) and phosphatase and tensin homolog (PTEN), respectively, transform PIP2 into PIP3 and vice versa. The phospholipids are permanently bound to the inner face of the cell membrane, while PI3K and PTEN diffuse in the cell volume and are active only when they are adsorbed by the membrane. PI3K adsorption takes place through binding to receptors activated by the extracellular attractant signal. This way, the external attractant field is coupled to the inner dynamic of the cell. PTEN adsorption takes place through binding to the PTEN product, PIP2. This process introduces a positive feedback loop in the system dynamics [19].

In experiments, cells initially at rest are exposed to a sudden increase in the concentration of uniformly distributed extracellular signal and allowed to relax to equilibrium [19,23]. During this interval of time a complex relaxational dynamics towards the final polarized state is observed. PIP3 patches are visualized by the use of fluorescent PH-Crac, a molecule that binds to a PH-binding domain present on the PIP3 molecule. The increase in PIP3 in the

plasmamembrane signaling domain is accompanied by a corresponding decrease of PH-Crac from the cytosol: the decrease in cytosolic PH-Crac fluorescence is therefore a measure of the total amount of PIP3 in the membrane. A puzzling aspect here is that plasmamembrane polarization seems to take place in two distinct stages. The initial stimulation with cAMP induces a uniform but transient increase in plasmamembrane PIP3 levels, of the duration of approximately 10 s. A second increase in PIP3 levels takes place after $\sim 20 - 30$ s, but is now localized in isolated, fluctuating domains, that occupy only a fraction of the membrane surface.

The decay of the initial uniform PIP3 burst suggests that an adaptation mechanism is at work [24]. The origin of the adaptation is likely upstream of PI3K [25]. However, the origin of the subsequent birth of localized PIP3 spots remains unclear. During the whole process PTEN and PI3K colocalize with their products, respectively PIP2 and PIP3 [19]. Although the appearance of PIP3 patches is triggered by cAMP, their size is approximately independent on cAMP levels over a wide range of concentrations, suggesting that the patches are self-organizing structures triggered by cAMP [19]. PIP3 patches show a competitive growth dynamics, with large clusters growing at the expense of smaller ones.

Colocalization of enzymes with their products implies the existence of positive feedbacks involving PIP2 and PTEN, as well as PIP3 and PI3K. Biochemical data confirm the existence of a PIP2–PTEN positive feedback loop, due to a PIP2-binding domain of PTEN [26–29], and of a PIP3–PI3K positive feedback loop at least in part mediated by actin [24,30–32].

The structure of the PIP2–PIP3 signaling network has the form described in Fig. 6, which fits with the abstract scheme (1–8, Fig. 1) once we identify $\Phi^+ = \text{PIP3}$, $\Phi^- = \text{PIP2}$, $X = \text{PI3K}$, $Y = \text{PTEN}$.

To understand the origin of the two-stage plasmamembrane polarization dynamics we start by simulating a spatially homogeneous version of Model (1–8). We mimic the experimental conditions by switching on receptor activation at initial time. To take into account the initial transient adaptation we let the input signal $s(t)$ adapt in the experimentally observed time $\tau \sim 1$ min (Fig. 7). As discussed above, the evolution of the phospholipid
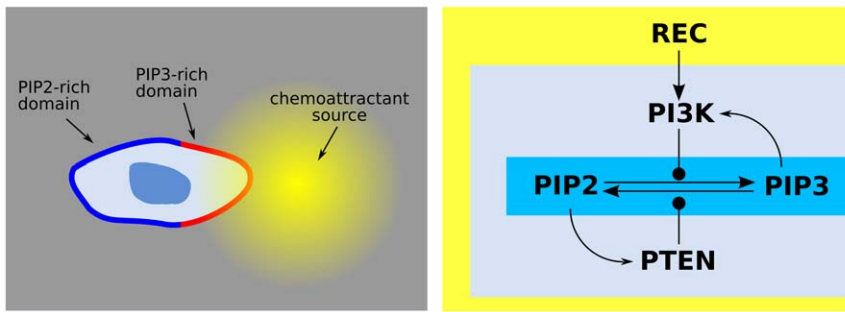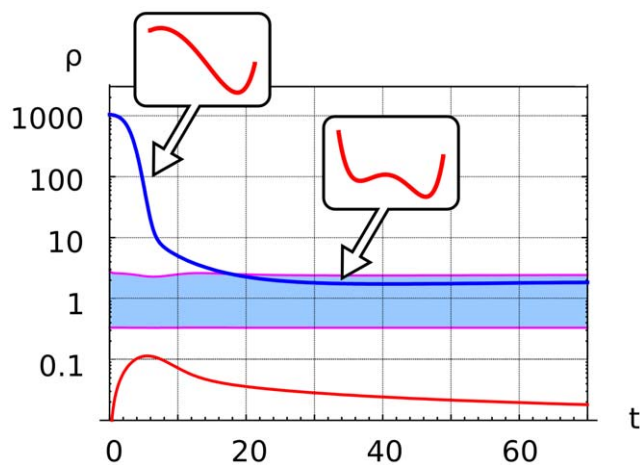
Figure 6. Model of chemotactic polarization. With respect to the abstract scheme in Fig. 1 we have the identification $\phi_+ = $ PIP3, $\phi_- = $ PIP2, $s = $ REC. The PIP3-rich domain corresponds to the presence of a high concentration of chemoattractant factor.
doi:10.1371/journal.pone.0030977.g006

concentration field is driven by the slow variation in time of the effective potential $V(\varphi)$, that follows the slow variation of the enzyme ratio $\rho \propto \text{PI3K}_f/\text{PTEN}_f$ (13, 19).

Receptor activation at $t = 0$ (Fig. 7, red line) induces a uniform increase of PI3K–PIP3 on the whole plasmamembrane, which corresponds to the appearance of a single potential well centered in the PIP3-rich region. The PI3K/PTEN enzyme ratio ρ decreases, corresponding to PI3K recruitment to the plasmamembrane and PTEN relocation to the cytosol (Fig. 7, red line). When the enzyme ratio crosses the boundary of the bistable region (Fig. 7, blue curve) the effective potential $V(\varphi)$ develops a secondary potential well centered in the PIP2-rich region.

The appearance of a secondary potential well follows from the increased concentration of cytosolic PTEN, which stabilizes the PIP2-rich phase. The potential barrier between the PIP2- and the PIP3-rich phase blocks further *uniform* increase in the PIP3 levels,

but still allows the formation of locally enriched PIP3-rich regions through a nucleation and growth dynamics, as described above.

In order to validate the present scenario we have simulated the full, spatially distributed system (1–8) by using a finite-element method, with $D = 0.02 \text{ m}^2/\text{s}$ and other parameters values reported from the literature (Table 2). Thermal and chemical reaction noise is taken into account by adding an additive random perturbation in the r.h.s. of (1, 2) (see Methods). Noise has the effect of creating germs of the PIP3-rich phase as localized, rare concentration fluctuations. In the simulation, before starting to stimulate cells with a uniform concentration of cAMP, the system is left to relax with zero signal until the levels of the relevant factors become stationary and the cell membrane becomes uniformly covered by the PIP2-rich phase (blue, Fig. 8b). The stimulation is switched on at time $t = 0$, when we also impose a 5% Gaussian noise on the uniform concentration background in order to mimic random inhomogeneities. In Fig. 8 we compare the experimental results reported in Ref. [19] with the simulations of model (1–8).

In both experiments (Fig. 8a) and simulations (Fig. 8b), switching on receptor activation leads to a transient increase in PIP3 concentrations (Fig. 8a). After a characteristic time of 5 s, PIP3 levels decrease by adaptation. After 30 s new PIP3 patches are nucleated and grow.

The kimograph in Fig. 8b shows the time evolution of simulated PIP3 levels along the major cell perimeter, while Fig. 9 shows this very same dynamics in 3D. Similarly to what observed in experiments, a transient, uniform increase in PIP3 levels is followed by a second regime where localized PIP3 patches phase nucleate and grow competitively in a PIP2-rich sea. In both the experiments and simulations, the speed of patch growth slows down with time. The features of the simulated dynamics are therefore completely consistent with the experimental data.

Simulation data reported in Fig. 9 hint at the 3D patch dynamics that we expect will be observed when dynamic 3D reconstructions of PIP3 patches in chemotactic experiments will become available.

Figure 7. We simulated a spatially homogeneous version of the Model. We mimic the experimental conditions by switching on receptor activation at initial time. The phospholipid concentration field is driven by the slow variation in time of the effective potential V, that follows the slow variation of the enzyme ratio $\rho \propto \text{PI3K}_{\text{free}}/\text{PTEN}_{\text{free}}$. Receptor activation at $t = 0$ (blue line) induces a uniform increase of PI3K, PIP3 on the whole plasmamembrane, which corresponds to the appearance of a single potential well centered in the PIP3-rich region. The enzyme ratio ρ decreases, corresponding to PI3K recruitment to the plasmamembrane and PTEN relocation to the cytosol (blue line). When the enzyme ratio crosses the boundary of the bistable region (light blue area) the effective potential V develops a secondary potential well centered in the PIP2-rich region.
doi:10.1371/journal.pone.0030977.g007

Epithelial polarization

In multicellular organisms, epithelial cells form layers separating compartments responsible for different physiological functions. At the early stage of epithelial layer formation, each cell of an aggregate defines a basal and an apical side. The *in vivo* process of epithelial morphogenesis is recapitulated in well established *in vitro* cell systems [33]: canine kidney cells are seeded in three-dimensional gels, where they divide and form cysts, *i.e.* hollow multicellular aggregates [33]. PIP2, PIP3 localization is central in the establishment of epithelial apico-basal polarity [34]. The apical

Table 2. Parameters used in the simulations of Eukariotic chemotaxis (Dictyostelium cells).
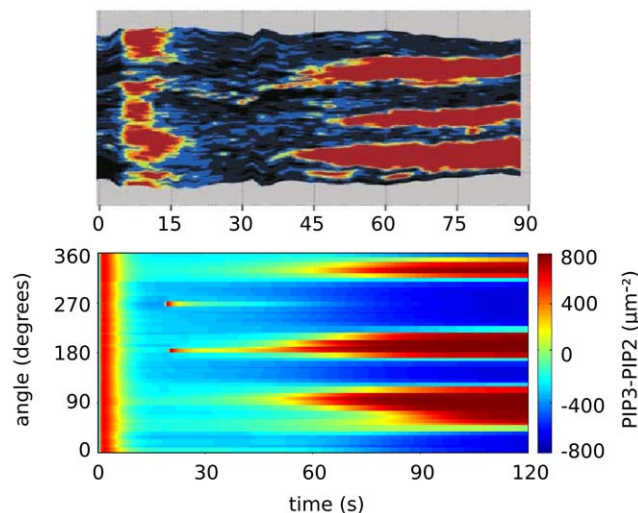
k_c	$1.00\,\mathrm{s}^{-1}$	k'_c	$1.00\,\mathrm{s}^{-1}$	k''_c	$0.10\,\mathrm{s}^{-1}$	c	$1000\,\mu\mathrm{m}^{-2}$
k_a	$0.006\,\mu\mathrm{m}^3\,\mathrm{s}^{-1}$	k'_a	$0.06\,\mu\mathrm{m}^3\,\mathrm{s}^{-1}$	k''_a	$0.006\,\mu\mathrm{m}^3\,\mathrm{s}^{-1}$	K	$500\,\mu\mathrm{m}^{-2}$
k_d	$0.10\,\mathrm{s}^{-1}$	k'_d	$0.10\,\mathrm{s}^{-1}$	k''_d	$0.01\,\mathrm{s}^{-1}$	x_T	$20\,\mu\mathrm{m}^{-3}$
K_d	$1.00\,\mu\mathrm{m}^{-3}$	K'_d	$1.00\,\mu\mathrm{m}^{-3}$	K''_d	$200.00\,\mu\mathrm{m}^{-3}$	y_T	$2\,\mu\mathrm{m}^{-3}$

We have simulated the full, spatially distributed system (1–8) by using a Finite Element Method, with the present parameter values, that were extracted from the literature.
doi:10.1371/journal.pone.0030977.t002

side facing the cyst lumen is characterized by high PTEN–PIP2 plasmamembrane levels, while the basolateral side is characterized by high PI3K–PIP3 levels (Fig. 10a). PTEN levels at the plasmamembrane are controlled by its binding to PIP2, thus realizing a positive feedback loop (Fig. 10b). PI3K levels in the membrane are controlled by its binding to cell-cell adhesive receptors, cadherins, and cell-matrix adhesive receptors integrins. To bind PI3K, cadherins must be activated by engagement with cadherins of a neighboring cell (C/M in Fig. 10b) [35]. PI3K is activated when associated with either activated cadherins or integrins. Since PIP3 stabilizes the activated form Cad [36], these interactions create a positive PI3K–PIP3 feedback loop, mediated by the existence of cell/cell contacts (Fig. 10).

Before polarization, cadherins and integrins are activated along the whole plasmamembrane and PIP3 uniformly prevails on PIP2 determining a stable PIP3-rich phase over the whole membrane. A local depletion of PI3K–PIP3 can be created if a large enough membrane area with disrupted cell-cell links is formed [37], thereby breaking the PI3K–PIP3 feedback loop (Fig. 6) and originating a germ of a PIP2-rich phase (Figs. 1b and 2). The

creation of this initial germ takes place by active transport of vesicles enriched in PTEN–PIP2 and antiadhesive factors to the midpoint of the mitotic spindle during the process of cell division [38,39]. After the formation of the initial PTEN–PIP2-rich germ, the PTEN–PIP2 feedback loop may locally prevail, inducing a PIP2 and PIP3 surface compartmentalization that splits the cell membrane in two regions, characterized by different chemical concentrations of the signaling molecules.

The structure of the PIP2–PIP3 signaling network in epithelial polarization has the form described in Fig. 10, which fits with the abstract scheme (1–8, Fig. 1) once we identify $\phi^+ = \mathrm{PIP3}$, $\phi^- = \mathrm{PIP2}, X = \mathrm{PI3K}, Y = \mathrm{PTEN}$. These are the same identification we used in the study of chemotactic polarization, but now with interactions and parameter values characteristic for epithelial polarity.

We have simulated Model (1–8) with parameter values compatible with the interactions described in Fig. 10 for the process of epithelial polarization (Table 3). At initial time the plasmamembrane is in a uniform PIP3-rich state. We than create a circular patch of radius r_0 of the PIP2-rich phase of radius r_0 and investigate its dynamics to check whether a stable polarization state is attained.

Patches smaller than a threshold radius $r_c \simeq 0.3\,\mu\mathrm{m}$ are dissolved by diffusion and thermal processes and do not impair the stability of the uniform PIP3-rich phase. Patches larger than r_c grow in time triggering the separation of the plasmamembrane surface in a PIP2-rich and a PIP3-rich region, and eventually reach an equilibrium, thus completing the separation into a PIP2-rich apical region and a PIP3-rich basolateral region (Fig. 11 and Ref. [37]). The critical radius for nucleation and the final PIP-patch size are functions of the PI3K/PTEN ratio ρ [37]. This fact suggests that the precise amount of PI3K and PTEN is a critical parameter for the establishement of epithelial polarity, providing an explanation for the experimental observation that deletion of a single PTEN allele can interfere with epithelial cell polarization and foster invasion of carcinoma cells [40].
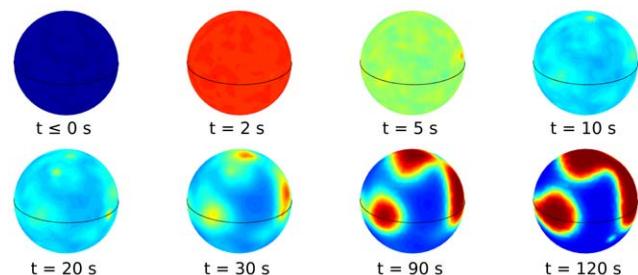

Figure 8. Kimograph for a simulation of the full, spatially distributed, chemotaxis system. In the simulation, before starting to stimulate cells with a uniform concentration of cAMP, the system is left to relax with zero signal until the levels of the relevant factors become stationary. Then, the stimulation is switched on at time $t = 0$, when we also impose a gaussian noise on the uniform concentration background in order to mimick random inhomogeneities. We compare the experimental results reported in Reference [19] with the simulations of model (1–8). The kimograph shows the time evolution of simulated PIP3 levels along the major cell perimeter. Time $t = 0$ in the simulation is to be compared with time 5 s in the experiment.
doi:10.1371/journal.pone.0030977.g008

Figure 9. The dynamics of the simulated 3D spatially distributed model for different times. The colorbar is the same as in Fig. 9, the major cell perimeter is the one considered in Fig. 9.
doi:10.1371/journal.pone.0030977.g009
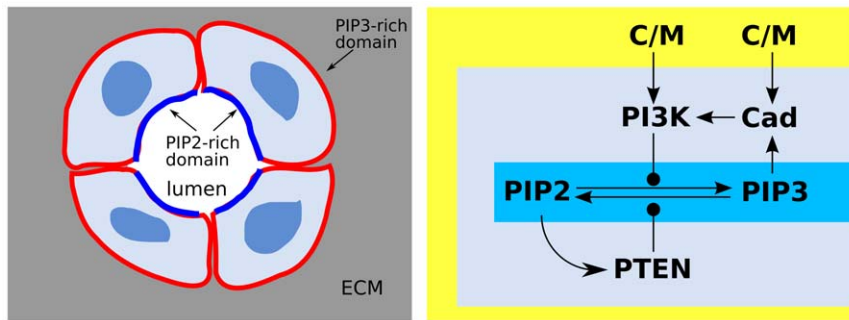
Figure 10. Model of epithelial polarization, with respect to the scheme in Fig. 1 we identify $\phi_+ = $ PIP3, $\phi_- = $ PIP2, $X = $ PI3K, $Y = $ PTEN, and $s = $ C/M. To bind PI3K, cadherins must be activated by engagement with cadherins of a neighboring cell. The PIP2, PIP3 localization is central in the establishment of epithelial apico-basal orientation.
doi:10.1371/journal.pone.0030977.g010

In the process of epithelial apico-basal symmetry breaking the roles of the PIP2- and PIP3-rich phases are reversed with respect to chemotaxis. More importantly, in chemotacting cells the tendency of the cell membrane to separate in two distinct signaling domains is triggered by shallow stimulation gradients, but can also take place spontaneously [4]. On the contrary, in order to preserve well-organized geometry of epithelia, the process of apico-basal symmetry breaking must be tightly regulated and cannot take place randomly [34]. It is worth observing here that a similar network topology may induce different dynamical behaviors, depending on parameter values. The model suggests that in chemotacting cells, the high sensitivity to shallow chemoattractant gradients depends on the existence of a low potential barrier separating the PIP2- and PIP3-rich phases. On the contrary, in the case of epithelial polarization a high potential barrier prevents the random occurrence of phase separation, making it a highly controlled process. In other words, our findings suggest that in eukaryotic chemotaxis germs of the PIP3-rich phase are created in the PIP2-rich phase by a process of *homogeneous nucleation* triggered by a random fluctuation, while in epithelial polarization a single germ of the PIP2-rich phase is created in the PIP3-rich phase by an active process, *i.e.* by a process of *heterogeneous nucleation*. Notably, this prediction is in agreement with the observation that lumen formation depends on the delivery at the plasmamembrane of exocytic vesicles containing PIP2 and apical proteins [41].

Budding yeast

Exposure to mating pheromone of haploid *Saccharomyces cerevisiae* cells results in polarized growth towards the mating partner [42]. Proteins involved in signaling, polarization, cell adhesion, and fusion are localized at the tip of the mating cell (shmoo) where fusion will eventually occur. Polarization involves localization of the small GTPase Cdc42 and of its guanine nucleotide exchange

factor (GEF), Cdc24. The expression of a constitutively activated form of Cdc42 is sufficient to cause polarization in otherwise nonpolarized cells [43].

During budding, polarization is independent from extracellular cues [42]. At the G1–S phase transition of each cell cycle, yeast cells polarize to form a bud in a direction specified by a remnant from the previous round of budding, the bud scar. Haploid cells form new buds adjacent to the previous bud scar. Diploid cells form new buds alternating between both cell poles, resulting in a bipolar budding pattern.

The Cdc24 GTPase is activated by Cdc42 via the scaffold protein Bem1, resulting in the amplifying feedback loop of Fig. 12. Moreover, several GTPase activating proteins (GAP), such as Rga2, can negatively regulate Cdc42 [44]. The structure of this signaling network fits with the abstract scheme (1–8, Fig. 1) once we identify $\phi^+ = $ Cdc42$^{\text{GTP}}$, $\phi^- = $ Cdc42$^{\text{GDP}}$, $X = $ Cdc24, $Y = $ Rga2.

It has been observed that intermittent, or "flickering" polarization may arise as a consequence of feedback mechanism as the one shown in Fig. 12 [45]. The model proposed in Ref. [45] is a limit case of our more general model, obtained by neglecting receptor activation and considering the limit of small number of bound Cdc42 molecules (see Supplementary Material Text S1). In this limit, $V(\varphi)$ has a single potential well and no stable polarization can be observed. However, intermittent signaling patches can still arise due to the interplay of chemical and reaction noise with the nonlinear feedback. In order to study the stochastic dynamics of intermittent patches we have simulated the full stochastic model (1–8) by Gillespie's algorithm (see Methods).

Fig. 13 shows the time evolution of simulated Cdc42$^{\text{GTP}}$ levels along a major cell cross section, while Fig. 14 shows the 3D behavior of intermittent Cdc42$^{\text{GTP}}$ patch formation. Values of the parameters used in the simulations are shown in Table 4. The

Table 3. Parameters used in the simulations of epithelial polarization.

k_c	$7.00\,\text{s}^{-1}$	k'_c	$7.00\,\text{s}^{-1}$	k''_c	$0.10\,\text{s}^{-1}$	c	$1000\,\mu\text{m}^{-2}$
k_a	$0.006\,\mu\text{m}^3\,\text{s}^{-1}$	k'_a	$0.06\,\mu\text{m}^3\,\text{s}^{-1}$	k''_a	$0.006\,\mu\text{m}^3\,\text{s}^{-1}$	K	$500\,\mu\text{m}^{-2}$
k_d	$0.10\,\text{s}^{-1}$	k'_d	$0.10\,\text{s}^{-1}$	k''_d	$0.01\,\text{s}^{-1}$	x_T	$20\,\mu\text{m}^{-3}$
K_d	$1.00\,\mu\text{m}^{-3}$	K'_d	$1.00\,\mu\text{m}^{-3}$	K''_d	$200.00\,\mu\text{m}^{-3}$	y_T	$2\,\mu\text{m}^{-3}$

We have simulated Model (1–8) with parameter values compatible with the interactions described in Fig. 10 for the process of epithelial polarization. At initial time the plasmamembrane is in a uniform PIP3-rich state. We then create a circular patch of the PIP2-rich phase of radius r_0 and investigate its dynamics to check whether a stable polarization state is attained.
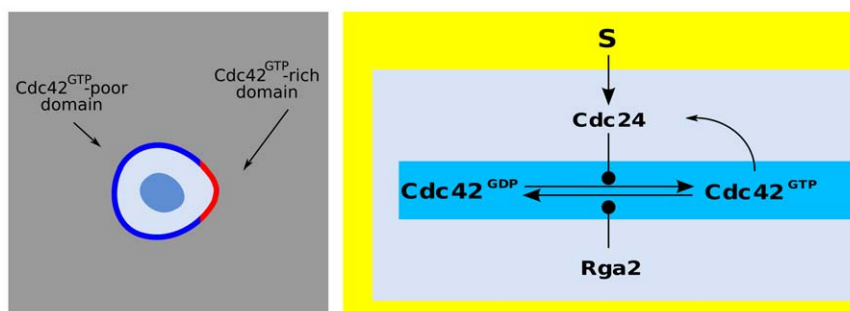doi:10.1371/journal.pone.0030977.t003
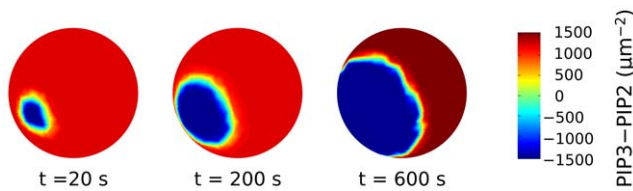
Figure 11. Growth of the PIP2-rich phase (blue lower patch). The color scale shows the gradation of PIP2 content: the color is the relative concentration difference between PIP3 and PIP2 at a given site. The system at initial time is in a uniform PIP3-rich phase (red), apart from an initial PIP2-rich seed germ of size larger than the threshold radius. Then, a PIP2-rich patch becomes apparent and its radius saturates to an equilibrium value.
doi:10.1371/journal.pone.0030977.g011

graphs of our realistic surface model are similar to those obtained in the one-dimensional model of Ref. [45]. It is worth observing here that intermittent, as opposed to stable, patch formation is here a consequence of the particular, small-concentration limit considered in [45]. However, our previous analysis shows that, if working in the appropriate parameter range, the signaling pathway described by Fig. 12 is bistable and capable of producing persistent polarized patches as those shown in Figs. 8, 9, in full agreement with experimental data [42].

Ras signaling domains

Ras GTPases are lipid-anchored G proteins which play a fundamental role in cell signaling processes [46]. Ras acts as a molecular switch with "on" (GTP-bound) and "off" (GDP-bound) states, the former promoting the activation of effector proteins. Ras activation is important for instance for the development of T and B lymphocytes and for their functions directed against invading pathogens [47]. Ras proteins have been observed to form dynamic non-overlapping domains (nanoclusters) in the inner leaflet of the plasmamembrane [48–50]. It has been shown that Ras clustering results in a prolonged immobilization at the plasmamembrane and in increased MAP-kinase activation [51].

The activation of Ras by receptor tyrosine kinases proceeds through the recruitment of the Ras-GEF Son of sevenless (Sos) to the plasma membrane [52,53]. It was discovered recently [53] that catalysis of Ras-GDP to Ras-GTP aided by SOS is 75-fold faster when a membrane associated SOS molecule is bound to Ras-GTP at an allosteric site. This mechanism introduces positive feedback regulation of Ras activation, which in the presence of slow diffusion, may result in clustering of activated molecules on the plasma membrane [12,48]. Moreover, several Ras-GAP proteins can negatively regulate Ras activation [54].
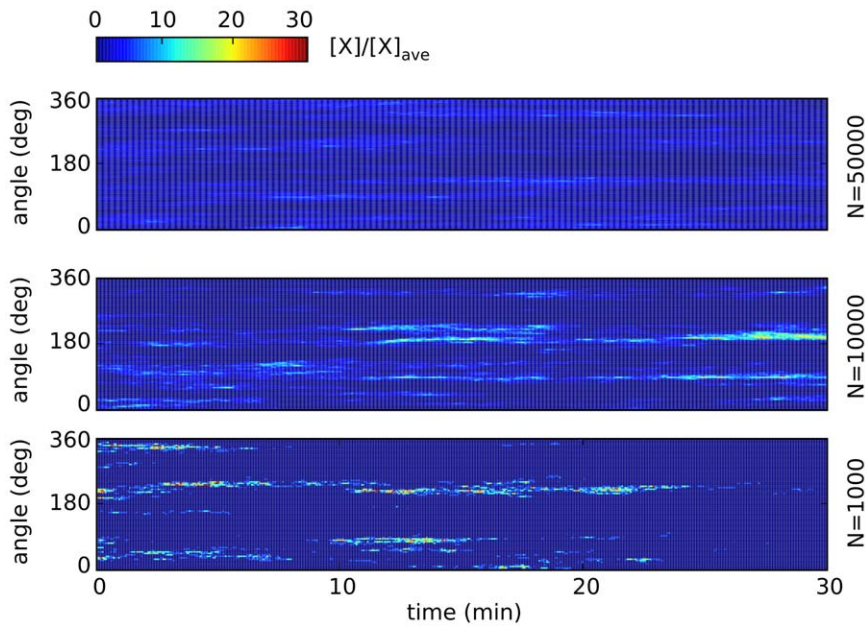
In Dictyostelium, Ras signaling domains have been observed at the leading edge of chemotaxing cells [25].

The Ras activation pathway (Fig. 15) is still another realization of the abstract scheme described in Fig. 1, with the identification $\phi^+ = \text{Ras}^{\text{GTP}}$, $\phi^- = \text{Ras}^{\text{GDP}}$, $X = \text{Sos}$, $Y = \text{Ras} - \text{GAP}$. In particular, the creation of germs of the ϕ^+-rich phase is expected to take place via the formation of small germs of the new phase by the action of random thermal and chemical fluctuations, as observed in [12]. Our previous analysis shows that the Ras-GDP/Ras-GTP system can support the formation of both intermittent nanoclusters, or stable signaling domains of Ras-GTP, depending on parameter values. The formation of patches of the ϕ^+-rich phase is expected to be intermittent outside of the bistable region II,III in Fig. 3, and generating stable signaling domains in the interior of these regions. Moreover, we expect that the role of the finite cytosolic reservoir of SOS should be central in tuning the cell plasma membrane towards coexistence of the φ^+-rich and φ^+-poor phases.

Discussion

Generation of spatio-temporally localized signaling domains is an ubiquitous feature of many cellular functions, such as chemotaxis, epithelial morphogenesis and mating. Interestingly, the organization of most of the corresponding molecular machineries involves molecules that exist in two alternative biochemical states, phosphatydilinositol and GTPases being prominent examples. The transition between these two states is typically controlled by the activity of a couple of counteracting enzymes. In addition, substrate-to-enzyme feedbacks can often generate hypersensitive responses. This ubiquitous pathway architecture can be formally described as a Goldbeter-Koshland hypersensitive module coupled with one or more reinforcing feedback loops. Here we have presented a general mathematical analysis of its properties.

Hypersensitivity has been considered for a long time as a way for a biochemical system to realize abrupt step responses to small variations in input concentrations. In the usual treatment, uniform spatial concentrations are considered. Here we have extended this approach to the case of spatially distributed, diffusive systems with reinforcing feedback loops. Our results show that in this context, Goldbeter-Koshland hypersensitivity can induce the separation of a biological system such as the cell plasmamembrane into distinct signaling domains. This simple principle appears of sufficient generality to explain the emergence of polarized domains in several basic biological settings, such as differentiation, proliferation, migration, and morphogenesis.

Figure 12. Model of cell polarization for budding yeast. With respect to the scheme in Fig. 1, we identify $\Phi^+ = \text{Cdc42}^{\text{GTP}}$, $\Phi^- = \text{Cdc42}^{\text{GDP}}$, $X = \text{Cdc24}$, $Y = \text{Rga2}$.
doi:10.1371/journal.pone.0030977.g012

Figure 13. Intermittent and persistent polarization obtained by simulation of model (1–8). In the graphs we plot concentrations of membrane-bound molecules along a 1 m thick cross section of the plasmamembrane *vs.* time, normalized with the average membrane concentration. Upper three rows: small number N of A-molecules (PTEN in Ref. [1], or Cdc24 in Ref. [45]). Intermittent polarization as shown here was already described in [1]. The graphs of our realistic surface model are similar to those obtained in Ref. [45] in the monodimensional case. Patches of signaling molecules randomly form and disappear. Observe that patches are the macroscopic counterpart of clans of signaling molecules, as defined in [45]. Parameter values were taken as follows: diffusivity of membrane-bound molecules is $D = 0.02$, m^2/s, [A] = 1, 10, 50 nM, the decay rate of A is adjusted in order to get 10% of A molecules bound to the plasmamembrane, all other parameters are as in [6,42].
doi:10.1371/journal.pone.0030977.g013

The idea that chemotactic cell polarization may result from the simple ingredients of bistability induced by a positive local feedback loop in a signaling network and global control induced by shuttling of enzymes between the cytosol and the membrane was advanced in our previous works [1,2,55]. Other authors have adopted similar models [11,13,56–60]. Alternative models include "local excitation – global inhibition" [24,61,62], Turing-like [65]
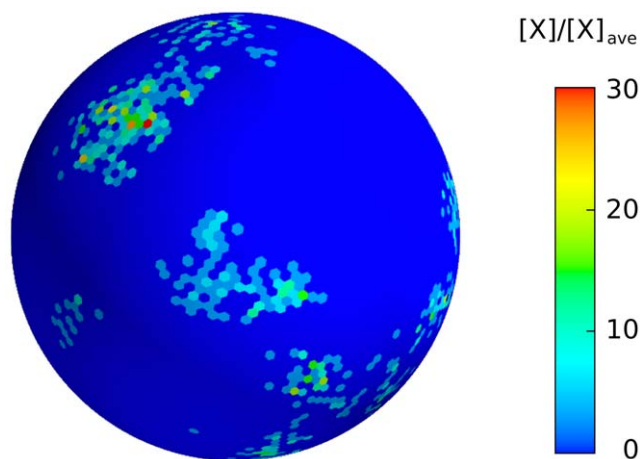
Figure 14. The 3D behavior of intermittent Cdc42[GTP] patches. The graphs of our realistic surface model are similar to those obtained in the one-dimensional model of Ref. [45]. It is worth observing here that intermittent, as opposed to stable, patch formation is here a consequence of the particular, small-concentration limit considered in [45].
doi:10.1371/journal.pone.0030977.g014

and excitable systems [66]. An extensive review of cell polarization models can be found in [63,64].

It is worth observing here that the coupling of local bistability and diffusion is an alternative way to produce patterning in an extended system, with respect to the better known mechanism of Turing instabilities [65,67,68]. The main difference is that Turing instabilities are linear instabilities of the uniform (mixed-phase) state. Instead, in our model an "energy" barrier has to be overcome to pass from the uniform state to the phase-separated state, similarly to what happens in the theory of phase separation in statistical physics. The mean-field, uniform state is stable, but a finite perturbation may break it. The finite perturbation may be produced either by random fluctuations (noise) in the system, or by an external perturbation, such as the introduction of a finite-size germ of one of the two phases. This way, the process of phase separation may be finely controlled by the signaling network.

Feedback loops participating in cell polarization may involve the actin cytoskeleton [24,30–32,69–71]. Such actin-mediated feedbacks may imply the active transport of signaling molecules along cytoskeleton filaments [69–71]. As long as the local geometry of actin filaments is neglected, active transport along cytoskeleton filaments may be taken into account in our model through renormalized values of the adhesion rates k_a (compare, e.g., Eq.s. 1–8, or Eq.s B.1–B.5 from Ref. [3], with Eq.s 1–4 from Ref. [71]). Different local geometries (e.g., astral or radial) of actin filaments in the proximity of the cell membrane may however facilitate or inhibit the development of instabilities leading to cell polarization [71,72]. These effects are expected to be particularly relevant if polarization is driven by Turing-like instabilities. In our bistable scenario, the effect of local inhomogeneities in the distribution of signaling molecules in the proximity of the cell membrane has still to be investigated.

Table 4. Parameters for simulations of budding yeast.

k_c	$50\,\mathrm{s}^{-1}$	k'_c	$0\,\mathrm{s}^{-1}$	k''_c	$0.1\,\mathrm{s}^{-1}$	c	$1000\,\mu\mathrm{m}^{-2}$
k_a	$0.01\,\mu\mathrm{m}^3\,\mathrm{s}^{-1}$	k'_a	$0\,\mu\mathrm{m}^3\,\mathrm{s}^{-1}$	k''_a	$0.1\,\mu\mathrm{m}^3\,\mathrm{s}^{-1}$	K	$500\,\mu\mathrm{m}^{-2}$
k_d	$0.10\,\mathrm{s}^{-1}$	k'_d	$0\,\mathrm{s}^{-1}$	k''_d	$0.1\,\mathrm{s}^{-1}$	x_T	$1-50\,\mu\mathrm{m}^{-3}$
K_d	$10\,\mu\mathrm{m}^{-3}$	K'_d	$0\,\mu\mathrm{m}^{-3}$	K''_d	$1\,\mu\mathrm{m}^{-3}$	y_T	$1\,\mu\mathrm{m}^{-3}$

Exposure to mating pheromone of haploid *Saccharomyces cerevisiae* cells results in polarized growth towards the mating partner. Proteins involved in signaling, polarization, cell adhesion, and fusion are localized at the tip of the mating cell (shmoo) where fusion will eventually occur. Polarization involves localization of the small GTPase Cdc42 and of its guanine nucleotide exchange factor (GEF), Cdc24. The expression of a constitutively activated form of Cdc42 is sufficient to cause polarization in otherwise nonpolarized cells.
doi:10.1371/journal.pone.0030977.t004

It has been recently shown that a bistable scenario for diffusible signaling molecules satisfactorily accounts for the polarization of fertilized oocytes, and for the flow of actomyosin cell cortex that is observed in the process, provided that the polarization pathway is properly coupled to the mechanics of membrane advection [73].

It is important to notice that a definitive assessment of the roles of Turing vs. bistable mechanisms in cell polarity can not be done by purely theoretical means. For instance, the mathematical description of the same signalling pathway may involve either nonlinearities leading to bistable behavior, if Michaelis-Menten saturation terms are taken into account to describe enzymatic kinetics (as we did here), or to Turing-like systems [65] if reactions are believed to be working in the non-saturating regime. Therefore, the Turing vs. bistability alternative can be ultimately solved only by performing accurate, targeted experiments.

Our model is simple enough to be studied by analytical methods, that in particular allow to derive a phase diagram showing the region of parameters where the coexistence of two signaling plasmamembrane domains is allowed. The dynamics leading to cell polarization can then be studied by introducing an *effective energy function* which encodes many of the qualitative and quantitative properties of the real process. This fact allows to draw a useful analogy with physical processes, such as the formation of precipitate from a supersaturated solution, and to take advantage of a well-developed mathematical theory of their dynamical properties. The main feature emerging from this analysis is that the system dynamics depends only on robust properties of the pathway architecture, such as bistability and self-tuning, and not on the precise values of microscopic details such as diffusion and chemical rate constants, or the identity of individual biochemical factors. This unified picture suggests that polarization phenomena observed in apparently distant biological models are sharing a set of common features.

Our theoretical framework leads to well-defined predictions about the polarized response of eukaryotic cells under both uniform and gradient stimulation conditions. To validate these predictions it would be necessary to systematically collect time-lapse, 3D microscopy data of signaling patches induced by controlled space-time extracellular stimulation patterns, such as those that can be realized by computer-controlled microfluidics.

Such measurements should be performed also by modulating the cellular levels of X and Y enzymes, e.g. by plasmid or virus-mediated overexpression as well as by gene silencing. Our theory suggests that when a cell is uniformly stimulated, the dynamic of signaling domains should show similar features in different biological models: at appropriate stimulation levels, signaling domains should appear as small intermittent spots that coarsen in time in a process where larger domains grow at the expense of smaller ones, finally reaching a configuration characterized by a single polarized cap.

A threshold in the stimulation levels is expected to separate a dynamics characterized by a "sea" of intermittent, small signaling domains (below threshold) and the above-mentioned coarsening dynamics leading to a single polarized cap (for above threshold stimulation levels). It is worth observing here that at low stimulation levels the signaling mechanism can be influenced by autocrine stimulation loops, which must therefore be accurately monitored.

The dynamics of signaling patches under gradient stimulation conditions is predicted to be quite similar to the dynamics observed under uniform stimulation conditions, except that polarization times should be much shorter and the direction of polarization should be aligned with the direction of the stimulation gradient.

Methods

The diffusion on the plasmamembrane has been simulated with a Finite Element Method for the Laplace-Beltrami operator and a suitable discretization of the spherical surface. The resulting ODE
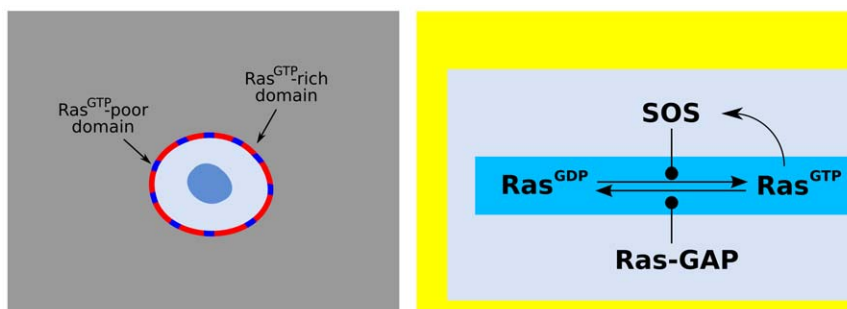
Figure 15. Ras activation pathway. With respect to the scheme in Fig. 1., we identify $\Phi^+ = \mathrm{Ras}^{GTP}$, $\Phi^- = \mathrm{Ras}^{GDP}$, $X = \mathrm{Sos}$, $Y = \mathrm{Ras\text{-}GAP}$.
doi:10.1371/journal.pone.0030977.g015

system has been approximated by using a Runge-Kutta stiff solver [74].

In the simulation of eukaryotic chemotaxis, noise intrinsic in the reaction-diffusion system is taken into account by adding an additive Poissonian random perturbation in the r.h.s. of (1, 2). In detail, nodes in the lattice are chosen randomly with rate $0.1\,\mathrm{s}^{-1}$ in time and with uniform probability in space and their state is set to $\phi = c$.

Reaction-diffusion kinetics has been simulated using Gillespie's method [75,76]. At time zero, a random number is generated to determine the next reaction or elementary diffusion process to occur, with a probability proportional to the corresponding W factor from Table 1. Then, the time is advanced as a Poissonian process with a rate again determined by the W factors. These steps are repeated iteratively until the desired simulation time is reached.

Supporting Information

Acknowledgments

Author Contributions

Conceived and designed the experiments: MS AV GN GS AG. Performed the experiments: MS AV GN GS AG. Analyzed the data: MS AV GN GS AG. Contributed reagents/materials/analysis tools: MS AV GN GS AG. Wrote the paper: MS AV GN GS AG.

References

1. Gamba A, De Candia A, Di Talia S, Coniglio A, Bussolino F, et al. (2005) Diffusion limited phase separation in eukaryotic chemotaxis. Proc Natl Acad Sci U S A 102: 16927–16932.
2. Gamba A, Kolokolov I, Lebedev V, Ortenzi G (2007) Patch coalescence as a mechanism for eukaryotic directional sensing. Phys Rev Lett 99: 158101–1–4.
3. Gamba A, Kolokolov I, Lebedev V, Ortenzi G (2009) Universal features of cell polarization processes. J Stat Mech 2009: P02019.
4. Wedlich-Soldner R, Li R (2003) Spontaneous cell polarization: undermining determinism. Nat Cell Biol 5: 267–70.
5. Kriebel PW, Barr VA, Parent CA (2003) Adenylyl cyclase localization regulates streaming during chemotaxis. Cell 112: 549–60.
6. Angeli D, Ferrell JE, Sontag ED (2004) Detection of multistability, bifurcations, and hysteresis in a large class of biological positive-feedback systems. Proc Natl Acad Sci U S A 101: 1822–1827.
7. Clarke BL (1980) Stability of complex reaction networks, volume 43 of Adv Chem Phys, pages 1–216.
8. Ferrell JE, Jr. (2002) Self-perpetuating states in signal transduction: positive feedback, double-negative feedback and bistability. Curr Opin Cell Biol 14: 140–8.
9. Goldbeter A, Koshland DE, Jr. (1981) An amplified sensitivity arising from covalent modification in biological systems. Proc Natl Acad Sci U S A 78: 6840–4.
10. Wilhelm T (2009) The smallest chemical reaction system with bistability. BMC Syst Biol 3: 90.
11. Beta C, Amselem G, Bodenschatz E (2008) A bistable mechanism for directional sensing. New J of Phys 10: 083015.
12. Das J, Kardar M, Chakraborty AK (2009) Positive feedback regulation results in spatial clustering and fast spreading of active signaling molecules on a cell membrane. J Chem Phys 130: 245102.
13. Mori Y, Jilkine A, Edelstein-Keshet L (2008) Wave-pinning and cell polarity from a bistable reaction-diffusion system. Biophys J 94: 3684.
14. Desai RC, Kapral R (2009) Dynamics of Self-organized and Self-assembled Structures Cambridge University Press.
15. van Kampen NG (2007) Stochastic Processes in Physics and Chemistry. North-Holland, thirdedition.
16. Flanders H (1989) Differential Forms – with Applications to the Physical Sciences. Dover, New York.
17. Ciliberto A, Capuani F, Tyson JJ (2007) Modeling networks of coupled enzymatic reactions using the total quasi-steady state approximation. PLoS Comput Biol 3: e45.
18. Evans LC (1998) Partial Differential Equations. American Mathematical Society.
19. Postma M, Roelofs J, Goedhart J, Loovers HM, Visser AJ, et al. (2004) Sensitization of Dictyostelium chemotaxis by phosphoinositide-3-kinase-mediated self-organizing signalling patches. J Cell Sci 117: 2925–35.
20. Bray AJ (1994) Theory of phase ordering kinetics. Adv Phys 43: 357–459.
21. Lifshitz IM, Slyozov VV (1961) The kinetics of precipitation from supersaturated solid solutions. J Phys Chem Solids 19: 35–50.
22. Landau LD, Lifshitz EM (1980) Statistical Physics (Part I), volume 5 of Course of Theoretical Physics. Pergamon Press, third edition.
23. Postma M, Roelofs J, Gadella TWJ, Visser AJ, et al. (2003) Uniform cAMP stimulation of Dictyostelium cells induces localized patches of signal transduction and pseudopodia. Mol Biol Cell 14: 5019–5027.
24. Janetopoulos C, Ma L, Devreotes PN, Iglesias PA (2004) Chemoattractant-induced phosphatidyli-nositol 3,4,5-trisphosphate accumulation is spatially amplified and adapts, independent of the actin cytoskeleton. Proc Natl Acad Sci U S A 101: 8951–6.
25. Kortholt A, Van Haastert PJ (2008) Highlighting the role of Ras and Rap during Dictyostelium chemotaxis. Cell Signal 20: 1415–22.
26. Campbell RB, Liu F, Ross AH (2003) Allosteric activation of PTEN phosphatase by phosphatidylinositol 4,5-bisphosphate. J Biol Chem 278: 33617–20.
27. Iijima M, Devreotes PN (2002) Tumor suppressor PTEN mediates sensing of chemoattractant gradients. Cell 109: 599–610.
28. Iijima M, Huang EY, Luo HR, Vazquez F, Devreotes PN (2004) Novel Mechanism of PTEN Regulation by Its Phosphatidylinositol 4,5-Bisphosphate Binding Motif Is Critical for Chemotaxis. J Biol Chem 16: 16606–16613.
29. Rahdar M, Inoue T, Meyer T, Zhang J, Vazquez F, et al. (2009) A phosphorylation-dependent intramolecular interaction regulates the membrane association and activity of the tumor suppressor PTEN. Proc Natl Acad Sci U S A 106: 480–5.
30. Wang F, Herzmark P, Weiner OD, Srinivasan S, Servant G, et al. (2002) Lipid products of PI(3)Ks maintain persistent cell polarity and directed motility in neutrophils. Nature Cell Biol 4: 513–518.
31. Weiner OD, Neilsen PO, Prestwich GD, Kirschner MW, Cantley LC, et al. (2002) A PtdlnsP3 and Rho GTPase-mediated positive feedback loop regulates neutrophil polarity. Nature Cell Biol 4: 509–512.
32. Meili R, Firtel RA (2002) Leading the way. Nature Cell Biol 4: E171.
33. Comer FI, Parent CA (2007) Phosphoinositides specify polarity during epithelial organ development. Cell 128: 239–40.
34. Bryant DM, Mostov KE (2008) From cells to organs: building polarized tissue. Nat. Rev Mol Cell Biol 9: 887–901.
35. Watton SJ, Downward J (1999) Akt/PKB localisation and 3′ phosphoinositide generation at sites of epithelial cell-matrix and cell-cell interaction. Curr Biol 9: 433–6.
36. Yap AS, Kovacs EM (2003) Direct cadherin-activated cell signaling: a view from the plasma membrane. J Cell Biol 160: 11–6.
37. Veglio A, Gamba A, Nicodemi M, Bussolino F, Serini G (2009) Symmetry breaking mechanism for epithelial cell polarization. Phys Rev E 80: 031919.
38. Rodriguez-Fraticelli AE, Vergarajauregui S, Eastburn DJ, Datta A, Alonso MA, et al. (2010) The Cdc42 GEF Intersectin 2 controls mitotic spindle orientation to form the lumen during epithelial morphogenesis. J Cell Biol 189: 725–38.
39. Zheng Z, Zhu H, Wan Q, Liu J, Xiao Z, et al. (2010) LGN regulates mitotic spindle orientation during epithelial morphogenesis. J Cell Biol 189: 275–288.
40. Carracedo A, Alimonti A, Pandolfi PP (2011) PTEN Level in Tumor Suppression: How Much Is Too Little? Cancer Res 71: 629–33.
41. Datta A, Bryant DM, Mostov KE (2011) Molecular Regulation of Lumen Morphogenesis. Curr Biol 21: R126–R136.
42. Bähler J, Peter M (2000) Cell Polarity, chapter Cell polarity in yeast, pages 21–77. Frontiers in molecular biology. Oxford Un. Press.
43. Wedlich-Soldner R, Altschuler S, Wu L, Li R (2003) Spontaneous cell polarization through actomyosin-based delivery of the Cdc42 GTPase. Science 299: 1231–5.
44. Yoshida S, Pellman D (2008) Plugging the GAP between cell polarity and cell cycle. EMBO reports 9: 39.
45. Altschuler SJ, Angenent SB, Wang Y, Wu LF (2008) On the spontaneous emergence of cell polarity. Nature 454: 886–890.
46. Bar-Sagi D, Hall A (2000) Ras and Rho GTPases: a family reunion. Cell 103: 227–38.
47. Genot E, Cantrell DA (2000) Ras regulation and function in lymphocytes. Curr Opin Immunol 12(3): 289–94.
48. Gurry T, Kahramanogullari O, Endres RG (2009) Biophysical mechanism for ras-nanocluster formation and signaling in plasma membrane. PLoS One 4: e6148.
49. Plowman SJ, Muncke C, Parton RG, Hancock JF (2005) H-ras, K-ras, and inner plasma membrane raft proteins operate in nanoclusters with differential dependence on the actin cytoskeleton. Proc Natl Acad Sci U S A 102: 15500–15505.
50. Prior IA, Muncke C, Parton RG, Hancock JF (2003) Direct visualization of Ras proteins in spatially distinct cell surface microdomains. J Cell Biol 160: 165–70.

51. Rotblat B, Belanis L, Liang H, Haklai R, Elad-Zefadia G, et al. (2010) H-Ras nanocluster stability regulates the magnitude of MAPK signal output. PLoS One 5: e11991.

52. Das J, Ho M, Zikherman J, Govern C, Yang M, et al. (2009) Digital signaling and hysteresis characterize ras activation in lymphoid cells. Cell 136: 337–51.

53. Freedman TS, Sondermann H, Friedland GD, Kortemme T, Bar-Sagi D, et al. (2006) A Rasinduced conformational switch in the Ras activator Son of sevenless. Proc Natl Acad Sci U S A 103: 16692–7.

54. Vigil D, Cherfils J, Rossman KL, Der CJ (2010) Ras superfamily GEFs and GAPs: validated and tractable targets for cancer therapy? Nat Rev Cancer 10: 842–57.

55. De Candia A, Gamba A, Cavalli F, Coniglio A, Di Talia S, et al. (2007) A simulation environment for directional sensing as a phase separation process. Sci STKE 2007(378): pl1.

56. Meier-Schellersheim M, Xu X, Angermann B, Kunkel EJ, Jin T, et al. (2006) Key role of local regulation in chemosensing revealed by a new molecular interaction-based modeling method. PLoS Comput Biol 2: e82.

57. Skupsky R, Losert W, Nossal RJ (2005) Distinguishing modes of eukaryotic gradient sensing. Biophys J 89: 2806–23.

58. Otsuji M, Ishihara S, Co C, Kaibuchi K, Mochizuki A, et al. (2007) A mass conserved reaction- diffusion system captures properties of cell polarity. PLoS Comput Biol 3: e108.

59. Arai Y, Shibata T, Matsuoka S, Sato MJ, Yanagida T, et al. (2010) Self-organization of the phosphatidylinositol lipids signaling system for random cell migration. Proc Natl Acad Sci U S A 107: 12399–12404.

60. Onsum M, Rao CV (2007) A Mathematical Model for Neutrophil Gradient Sensing and Polarization. PLoS Comput Biol 3: e36.

61. Krishnan J, Iglesias PA (2004) A modeling framework describing the enzyme regulation of membrane lipids underlying gradient perception in Dictyostelium cells. J Theor Biol 229: 85–99.

62. Ma L, Janetopoulos C, Yang L, Devreotes PN, Iglesias PA (2004) Two Complementary, Local Excitation, Global Inhibition Mechanisms Acting in Parallel Can Explain the Chemoattractant- Induced Regulation of PI(3,4,5)P3 Response in Dictyostelium Cells. Biophys 87: 3764–74.

63. Iglesias PA, Devreotes PN (2007) Navigating through models of chemotaxis. Curr Op Cell Biol 20: 1–6.

64. Jilkine A, Edelstein-Keshet L (2011) A comparison of mathematical models for polarization of single eukaryotic cells in response to guided cues. PLoS Comput Biol 7: e1001121.

65. Goryachev AB, Pokhilko AV (2008) Dynamics of Cdc42 network embodies a Turing-type mechanism of yeast cell polarity. FEBS Lett 582: 1437–43.

66. Hecht I, Kessler DA, Levine H (2010) Transient localized patterns in noise-driven reaction-diffusion systems. Phys Rev Lett 104: 158301.

67. Cross MC, Hohenberg PC (1993) Pattern formation outside of equilibrium. Rev Mod Phys 65: 851–1112.

68. Gierer A, Meinhardt H (1972) A theory of biological pattern formation. Kybernetik 12: 30–39.

69. Wedlich-Soldner R, Wai SC, Schmidt T, Li R (2004) Robust cell polarity is a dynamic state established by coupling transport and GTPase signaling. J Cell Biol 166: 889–900.

70. Marco E, Wedlich-Soldner R, Li R, Altschuler SJ, Wu LF (2007) Endocytosis optimizes the dynamic localization of membrane proteins that regulate cortical polarity. Cell 129: 411–22.

71. Hawkins RJ, Benichou O, Piel M, Voituriez R (2009) Rebuilding cytoskeleton roads: activetransport-induced polarization of cells.. Phys Rev E Stat Nonlin Soft Matter Phys 80: 040903.

72. Calvez V, Meunier N, Voituriez R (2010) A one-dimensional Keller–Segel equation with a drift issued from the boundary. Comptes Rendus Mathematique 348: 629–634.

73. Goehring NW, Khuk TP, Bois JS, Chowdhury D, Nicola EM, et al. (2011) Polarization of PAR Proteins by Advective Triggering of a Pattern-Forming System. Science.

74. Hairer E, Wanner G (2010) Solving ordinary differential equations II: Stiff and differential-algebraic problems Springer.

75. Gillespie DT (1977) Exact stochastic simulation of coupled chemical reactions. J Phys Chem 81: 2340–2361.

76. Schöll E (2000) *Stochastic Processes in Physics, Chemistry, and Biology*, volume 557 of *Lecture Notes in Physics*, chapter Nonlinear spatiotemporal patterns in globally coupled reaction-diffusion systems, pages 437–451. Springer.